

Supporting Information

Probing the evolution of conductivity and structural changes in vapor-F4TCNQ doped P3HT

Mark DiTusa¹, Garrett L. Grocke², Tengzhou Ma², Shrayesh N. Patel^{2*}

¹Department of Physics, ²Pritzker School of Molecular Engineering, University of Chicago, Chicago, Illinois 60637, USA

Contents

1. Pristine P3HT UV-Vis absorption fit with Spano model.
2. CV of F4TCNQ and P3HT
3. Vapor doping set up
 - A Sample holder for vapor doping set up
 - B Doping chamber for vapor doping set up
4. Vapor doping *in situ* conductivity data
 - A Vapor doping experiments with lower dopant temperature
 - B Renormalized plot comparing shape of doping curves with different dopant temperatures
 - C Vapor doping experiments with melt-recrystallized films
5. UV Vis data
 - A Plot of absorption from P3HT-F4TCNQ doped at 30 °C
 - B Plot of absorption from P3HT-F4TCNQ doped at 70 °C
6. Fit of UV-Vis absorption
7. GIWAXS images for doping P3HT-F4TCNQ at 0°C at 50 s intervals
8. GIWAXS images for doping P3HT-F4TCNQ at 30°C at 50 s intervals
9. GIWAXS images for doping P3HT-F4TCNQ at 70°C at 50 s intervals
10. Raman spectroscopy data
 - A Unnormalized spectra for 785 nm excitation doped at 0 °C
 - B Unnormalized spectra for 785 nm excitation doped at 70 °C

11. Wider view of 785 nm excitation Raman peak fitting

Table 1 List of peaks fit for Raman spectra

Table 2 785 nm excitation peak area doped at 0 °C

Table 3 785 nm excitation peak area doped at 30°C

Table 4 785 nm excitation peak area doped at 70°C

I. Spano Model Fit of Neat P3HT.

The Spano model was used to make estimate of percent of aggregate versus amorphous fractions in the P3HT used in this study. The model dictates that the absorption spectra of P3HT thin films in the ~2.0 eV to 3.0 eV range are comprised of low-energy π -stacking aggregate peaks and higher energy amorphous-fraction peaks. In order to determine the vibration bands for the aggregate portion, we utilize a Franck-Condon fit:

$$A_{\text{aggregate}} \propto \sum_{m=0} \left(\frac{S^m}{m!} \right) \times \left(1 - \frac{W e^{-S}}{2E_p} \sum_{n \neq m} \frac{S_n}{n! (n-m)} \right)^2 \times e^{(E-E_0 - mE_p - \frac{1}{2}WS^m e^{-S})^2 / 2\sigma^2}$$

Where A is the absorption of the aggregates as a function of photon energy, E ; S is the Huang-Rhys factor, which represents the overlap between individual vibrational states (we assume this to be 1 for this fit); m corresponds to different vibrational energy levels; $E_p = 0.179$ eV the energy of the C=C symmetric branch mode in P3HT; the three fitting parameters are: W , the exciton bandwidth; E_0 , the transition energy; and σ , the energetic disorder, which in this case is the Gaussian width of the absorption peaks. The peaks generated by this Franck-Condon fit can be seen in figure S1B: the individual peaks are red with dotted lines, and the summation the solid red line, which appears to fit the shoulder from ~2.0 eV to 2.5 eV in the absorption well. The amorphous fraction was taken to be the higher energy region, obtained by subtracting the aggregate absorption calculated from the absorption from the experiment. The percent aggregate is calculated from this fit by taking the integrated area of the aggregate peaks to the amorphous peaks, and this was found for this fit to be roughly 37%. A Matlab fit program was used to perform the Spano fit as described by Dong *et al.*¹

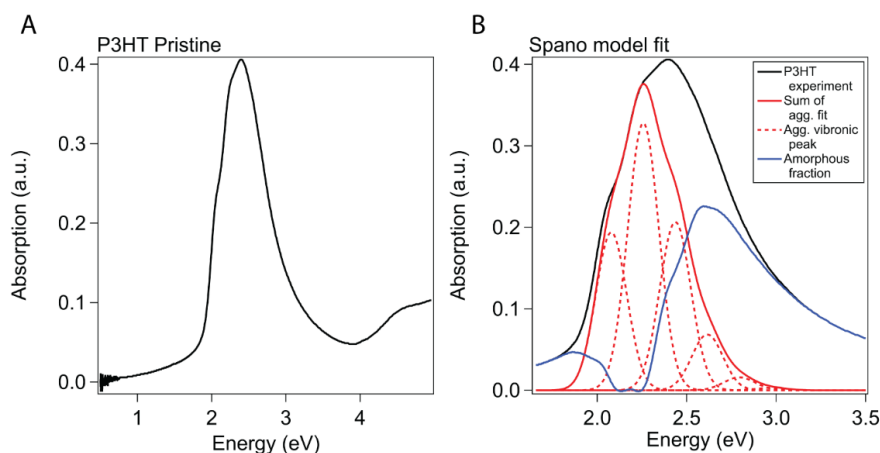


Figure S1. (A) UV-Vis-NIR of neat P3HT thin film. (B) Spano model fit.

II. Cyclic voltammetry of P3HT and F4TCNQ.

Cyclic voltammetry (CV) was performed using a Biologic SP200 potentiostat in a standard 3-electrode configuration. Testing was performed in an anhydrous, degassed acetonitrile solution with a 0.1 M tetrabutylammonium hexafluorophosphate supporting electrolyte concentration at a scan rate of 0.1 V/s. A silver wire in 0.01 M AgNO₃ and 0.1 M supporting electrolyte served as a reference electrode, and a platinum wire was used as a counter electrode. Ferrocene purified by sublimation was used as an internal standard. All experiments were performed in a dry argon glove box. F4TCNQ was dissolved directly in acetonitrile at 0.01 M concentration. P3HT was spin coated onto an ITO-coated glass slide according to the procedure described in the methods section in the main manuscript. Ionization energy (IE, HOMO) of the polymers and electron affinity (EA, LUMO) of the dopants were determined by comparison against the ferrocene couple (5.1 eV), as described here:

$$IE = q(E_{ox} + 5.1 - E_{F,ox})$$
$$EA = q(E_{red} + 5.1 - E_{F,red})$$

where q is the fundamental charge of an electron, E_{red} is the reduction potential of F4TCNQ, and $E_{F,red}$ is the oxidation potential of ferrocene. Onset potentials were calculated by regressing the rising slope of the oxidation peak to the intersection point of the system background current. The linear regression and background current are seen as straight lines in the CV plot for P3HT. F4TCNQ's LUMO level was calculated by this method to be 5.25 eV, and the HOMO for P3HT was calculated by this method to be approximately 5.1 eV.

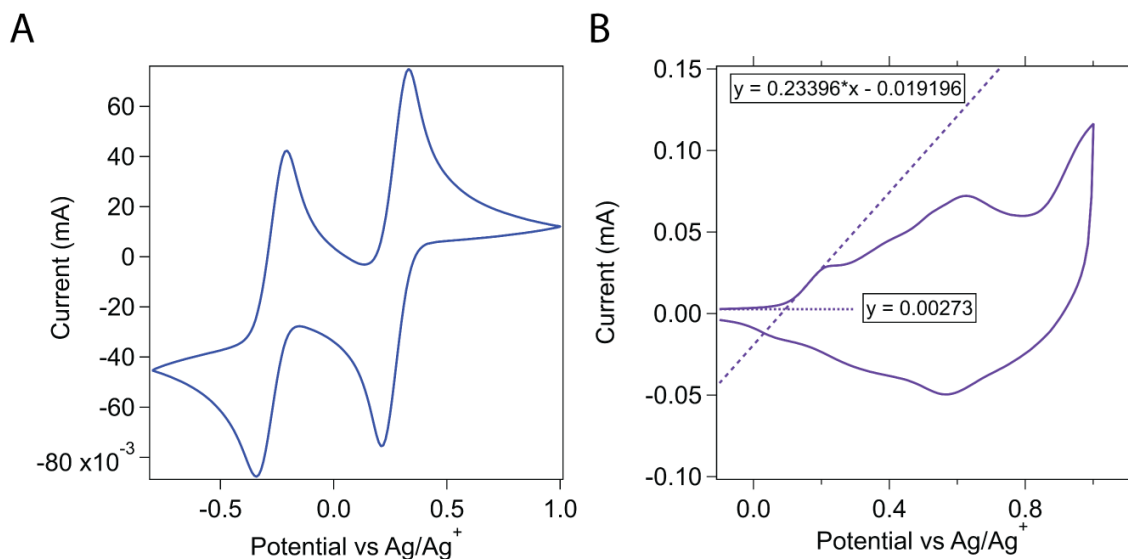


Figure S2. (A) CV of F4TCNQ. (B) CV of P3HT.

III. Vapor doping setup and experimental details

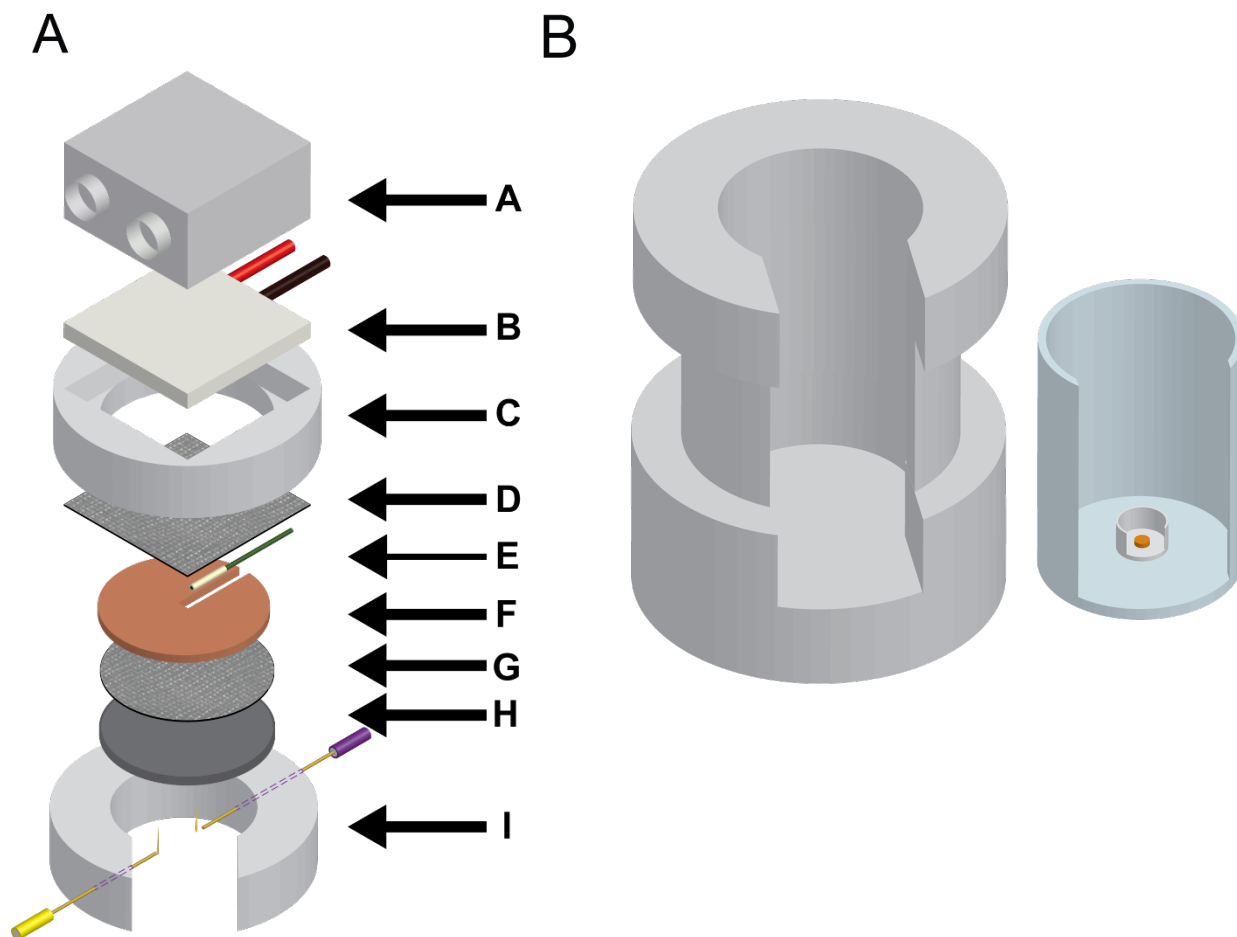


Figure S3. 3D renders of sample holder and doping chamber. For sample holder (S1A): A- aluminum water-cooling block. B- Peltier thermoelectric module. C- Peltier module housing. D- thermally conductive adhesive. E- thermistor for monitoring sample temperature. F- copper heat spreader. G- thermally conductive adhesive. H- silicon wafer sample base. I- retention ring with retaining electrode probes. For doping chamber (S1B), a stainless steel chamber (left) jackets a quartz glass insert (right), which holds an alumina crucible with dopant pellet in a recess. A thermocouple in the base of the doping chamber measures the temperature of the doping chamber, allowing for control over the doping temperature.

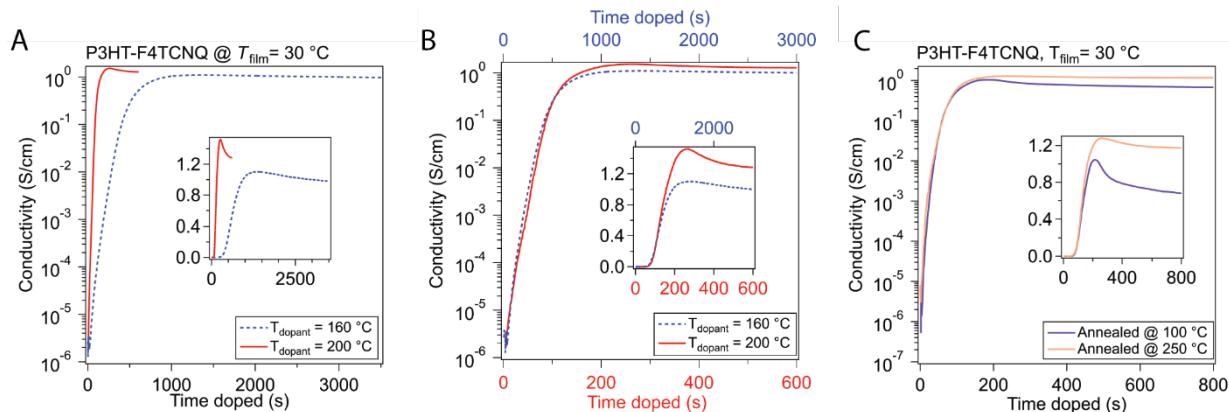


Figure S4. *In situ* conductivity curves for different dopant temperatures and processing methods. (A) F4TCNQ was set to 200 °C for the entirety of the F4TCNQ doping experiments shown in Figure 2 of the main manuscript. An experiment was conducted in order to test how lowering the dopant temperature, and hence the sublimation rate, would affect the conductivity curve. When doped with F4TCNQ sublimed at 160 °C, the doping went slower; however, when corrected for sublimation rate (dividing by five), as shown in (B), the two curves agreed well, showing a similar curve shape. This is in rough agreement with our thermogravimetric analysis experiments to test for sublimation rate; the rate for F4TCNQ at 160 °C was one sixth that at 200 °C. (C) Samples in the main manuscript were annealed below their recrystallization temperature. Experiments were conducted to see if recrystallizing the P3HT at 250 °C would result in different doping curves. Although the σ_{\max} appear different, this difference in σ_{\max} was standard between samples from different batches of P3HT solution; it appears that although the recrystallized sample starts at a higher σ , their σ_{\max} are comparable. The timing looks similar, with the recrystallized P3HT showing more stability after the maximum conductivity.

IV. UV-Vis-NIR

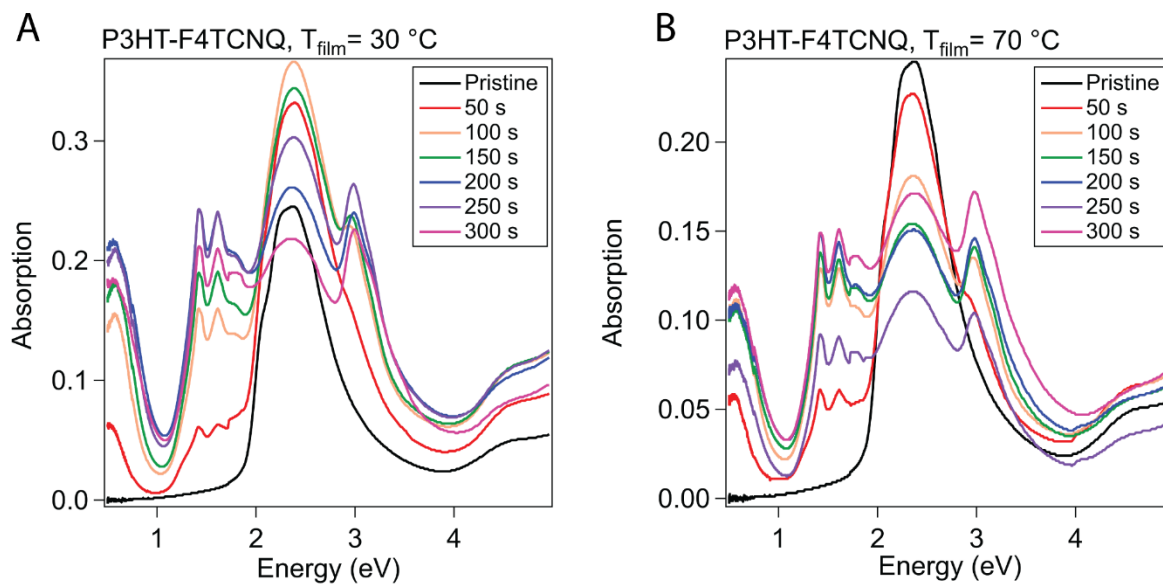


Figure S5. Absorption of P3HT-F4TCNQ at 30 °C and 70 °C. Absorption measurements were conducted on P3HT-F4TCNQ films doped to the levels shown in fig. 3 (0 s to 300 s at 50 s intervals). (A) shows the spectra for films doped with the film held at 30 °C, and (B) at 70 °C.

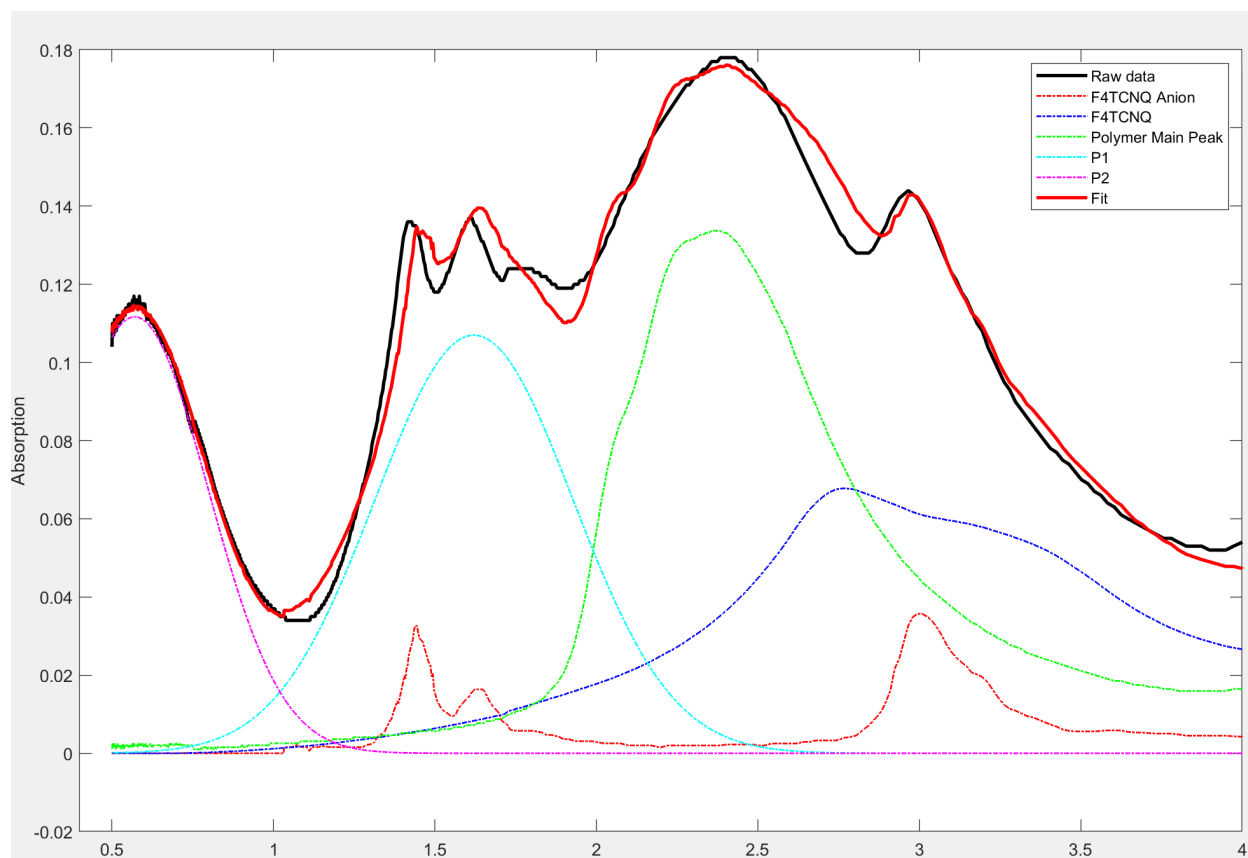


Figure S6. Fit of UV-Vis absorption. Description of peaks adapted from Hynynen, Kiefer and Müller.² F4TCNQ anion, polaron peaks 1 and 2 were taken from the same paper. The F4TCNQ neutral peak was obtained from our own absorption measurements on vapor-deposited F4TCNQ. The ratio between the fitted polaron 1 peak (labeled P1 here) and the polymer neutral peak (labeled polymer main peak here) is what is used in fig. 4 in the main manuscript.

V. Grazing Incidence Wide Angle X-ray Scattering (GIWAXS) data

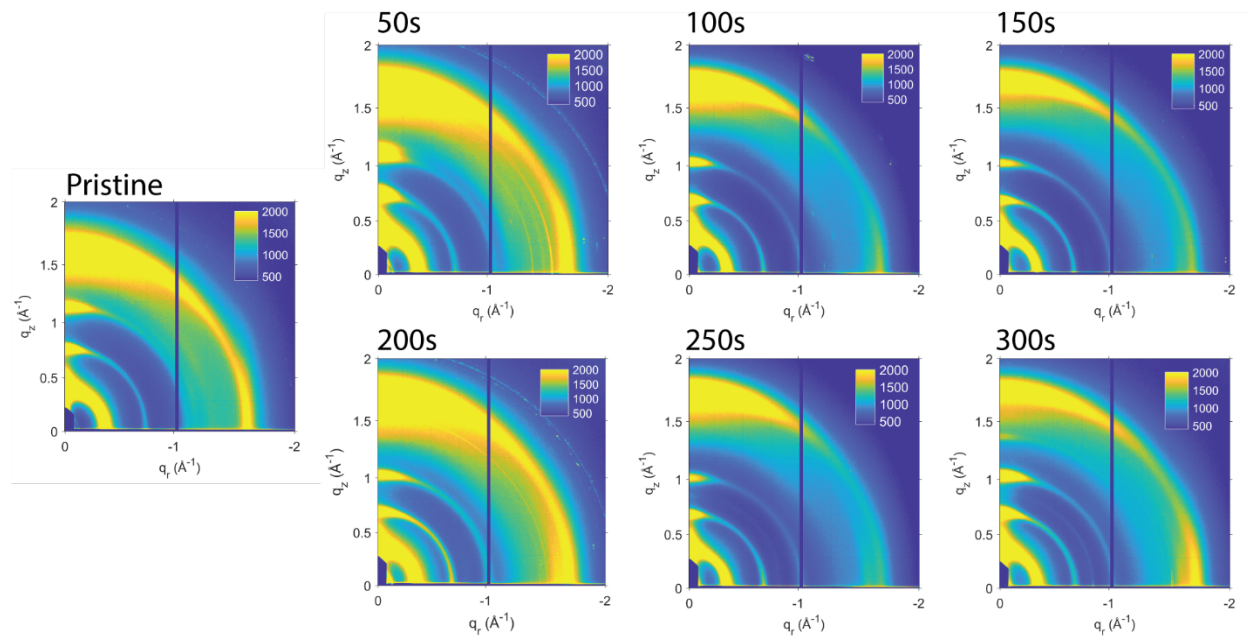


Fig. S7. P3HT-F4TCNQ scattering, doped at 0°C.

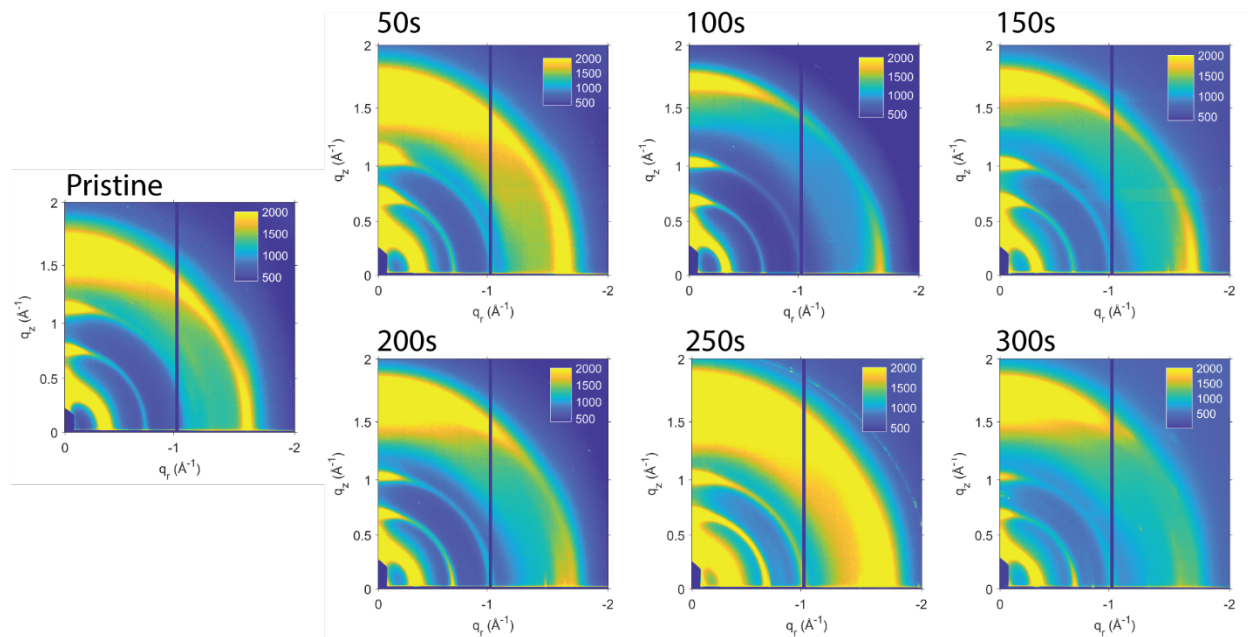


Fig. S8. P3HT-F4TCNQ scattering, doped at 30°C.

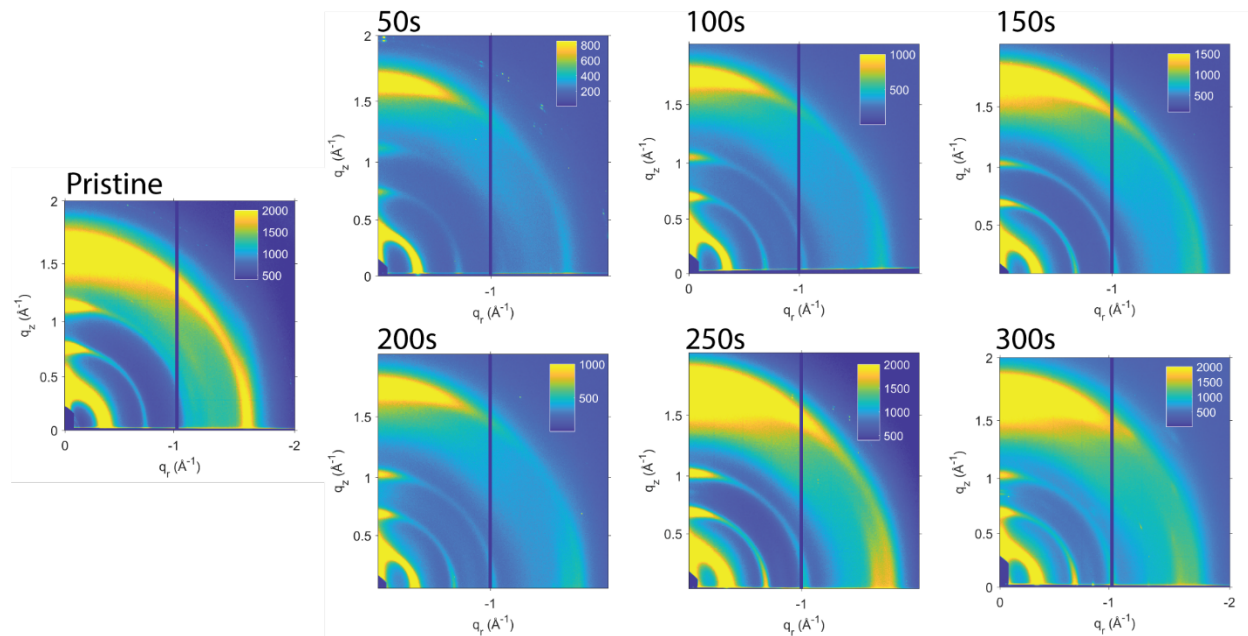


Fig. S9. P3HT-F4TCNQ scattering, doped at 70°C.

VI. Raman spectroscopy and fitting

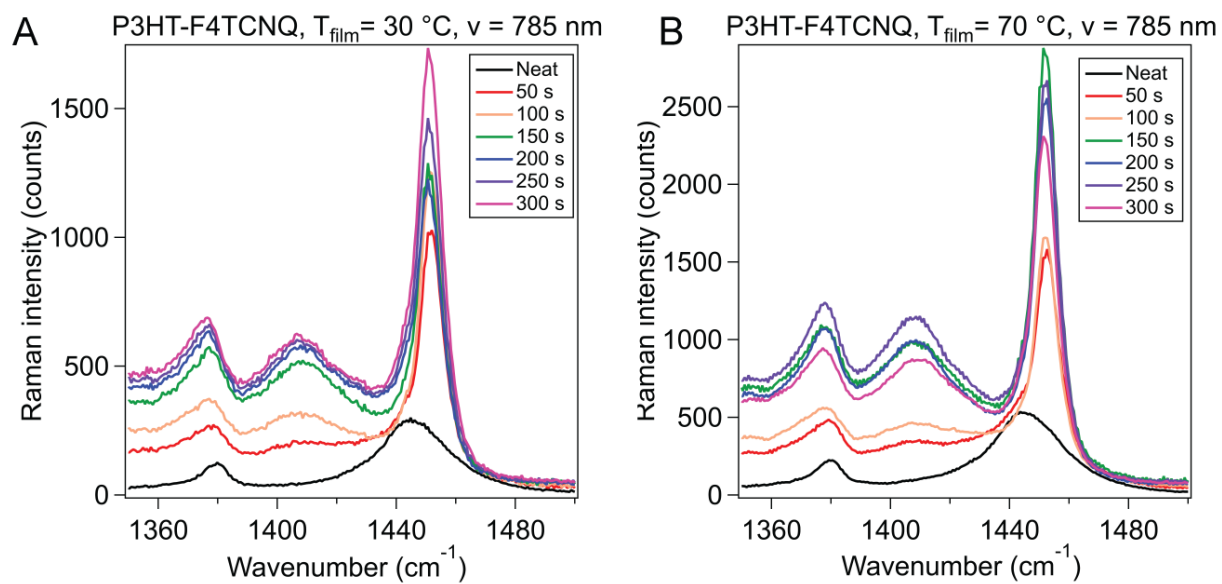


Figure S10. Raman spectra of P3HT-F4TCNQ excited by 785 nm laser @ 0 and 70 $^{\circ}\text{C}$. Raman spectra collected on P3HT doped to films doped with F4TCNQ from 0 s to 300 s at 50 s intervals. Film were doped at (A) 0 $^{\circ}\text{C}$ and (B) 70 $^{\circ}\text{C}$, and excited by 785 nm laser.

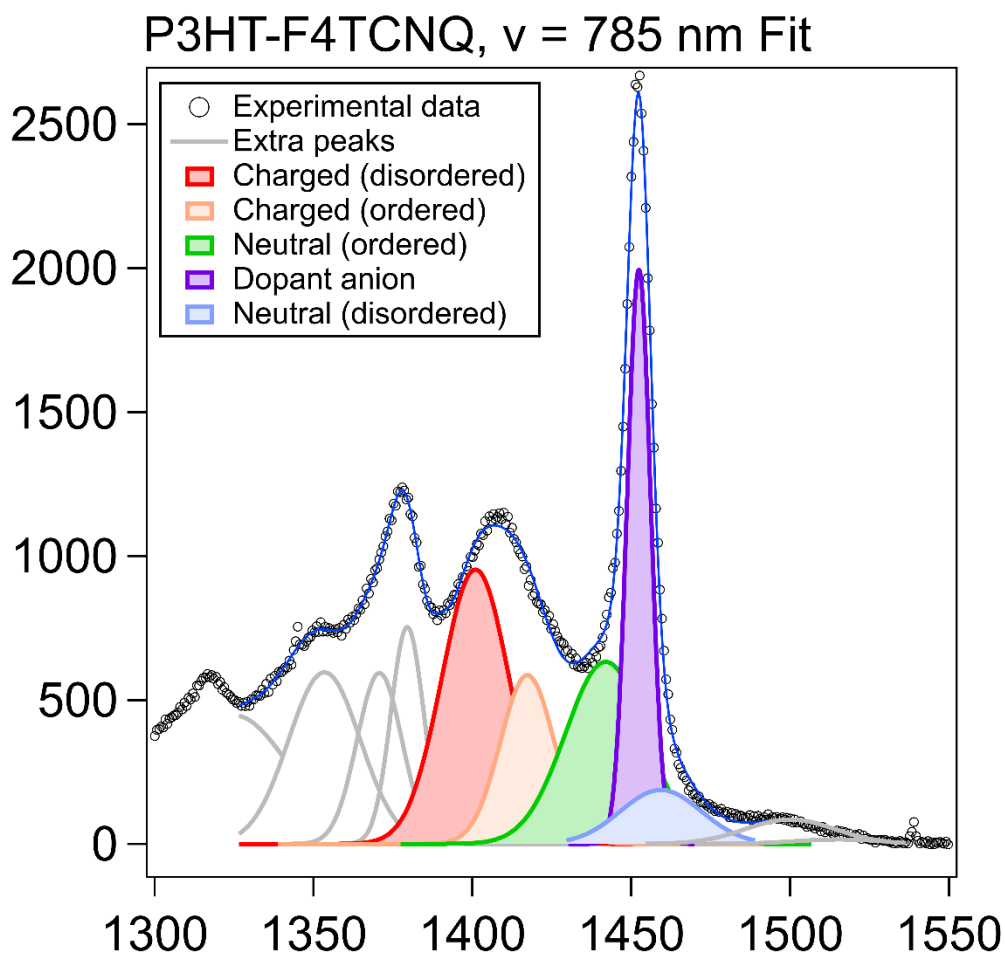


Figure S11. Wider view of 785 nm excitation Raman peak fitting. A broader view of the peak fitting done for a 785 nm excitation Raman spectrum. Peaks colored in were used for the analysis seen for the bar graphs in the main manuscript. Grey peaks were included to fit the rest of the data and allow for accurate tracking of the peaks of main interest.

Discussion of Raman spectrum deconvolution and analysis

Our analysis centers on deconvolution of the main C=C stretching peaks in the region from 1400 cm^{-1} to 1460 cm^{-1} , which we attribute first to the work of Nightengale *et al.*, but also point towards work by Degousée *et al.* and Dyson *et al.* as exemplary works utilizing this style of analysis.³⁻⁵ In particular, we utilize the fact that the C=C symmetric stretch shifts to shorter wavelength for chains with a higher conjugation length. Although this order is probed at the level of a bond on an individual chain, domains in P3HT are such that there are crystalline domains with a higher

proportion of long-conjugation length chains, and amorphous domains with a greater proportion of low conjugation length chains, and hence we take ratio of higher conjugation length chains to lower conjugation length chains as a measure of how ordered or disordered the material is as a whole.

When we excite the film for Raman spectroscopy using a 785 nm laser, we preferentially excite the charged regions of the film, as this wavelength/energy corresponds to the P2 absorption in the UV Vis (as seen in fig. S6). This resonance strengthens the contribution to the Raman spectrum from the charged parts of the films and allows for deconvolution of the charged C=C stretching peak seen at a slightly lower wavenumber, around 1410 to 1420 cm^{-1} , into charged ordered and charged disordered populations. The lower peak center wavenumber compared to the neutral portions of the film is due to a higher planarity of the polymer upon introduction of charge carriers into the system; the fact that the disordered charged phase has a peak centered around a lower wavenumber is due to a larger change in bond length locally around the charge carrier in the amorphous (disordered) domain than the ordered domain.

When taken as a whole, we argue that fitting the C=C symmetric peak as deconvoluted into charged disordered ($\sim 1401 \text{ cm}^{-1}$), charged ordered ($\sim 1420 \text{ cm}^{-1}$), neutral ordered ($\sim 1447 \text{ cm}^{-1}$), and neutral disordered ($\sim 1462 \text{ cm}^{-1}$) Gaussian peaks allows us to track the evolution of doping within the ordered and amorphous phases of our polymer separately. We achieve this by fitting and tracking how these peaks change over the course of our timepoints, from the undoped film, to films doped 300 s by F4TCNQ.

In order to accurately track the evolution of these peaks, we use the peak positions and FWHM suggested by Nightingale *et al.* for these modes, but set constraints of roughly $\pm 3 \text{ cm}^{-1}$ to $\pm 5 \text{ cm}^{-1}$, dependent on the variance in peak positions reported for P3HT by Nightingale *et al.* and Degousée *et al.* We believed that constraining the FWHM, rather than fixing, would also represent the changing population of conjugation lengths in the individual phases more accurately. The FWHM for all C=C modes were constrained between 0 and 50 cm^{-1} , except for the charged disordered phase, which was constrained between 0 and 20 cm^{-1} , to fit how these peaks were constrained prior by Degousée *et al.*

F4TCNQ anion was also confirmed to have a peak present within the range that we were deconvolution for peaks, sharply resolved at around 1452 cm^{-1} . This peak was fit in order to be able to accurately deconvolute those peaks resulting from the polymer and that of the dopant.

The window of the Raman spectra that were fit roughly spanned from 1250 cm^{-1} to 1600 cm^{-1} . Gaussians with FWHM between 0 and 20 cm^{-1} that were given a constraint on location in a range of 20 cm^{-1} were fit in order to account for all Raman counts between the fit range and produce accurate fit data for the four main peaks, including the C-C stretching around 1380 cm^{-1} . The peak locations and areas under the curve for the four C=C modes are included comprehensively in the tables below for this analysis and can be seen in figure S11 for an example fitting.

Table S1. Approximate peak location and widths for Raman fits with both excitation lasers

P3HT-F4TCNQ excited by 785 nm		
Peak origin	Peak Location (cm^{-1})	FWHM (cm^{-1})
Charged, disordered fraction	1399 - 1405	20
Charged, ordered fraction	1415 - 1425	28 - 38
Neutral, ordered fraction	1442 - 1447	22
Dopant anion	1451 - 1453	5 - 8
Neutral, disordered fraction	1455 - 1462	23 - 35

Peak locations for the ordered and disordered fractions of P3HT that were charged and neutral, listed in the table above, were used for the fits in the tables below as starting points. These peaks can be seen labeled in the main manuscript in figure 5B and 5E. These peak locations and widths were sourced from a similar analysis done by Nightingale *et al.*⁴

Table S2. Fit of Raman spectra for P3HT-F4TCNQ excited by 785 nm at 0°C

P3HT-F4TCNQ 0 °C										
	Charged Disordered		Charged Ordered		Neutral Ordered		Dopant Anion		Neutral Disordered	
Time doped (s)	Peak location (cm^{-1})	Area	Peak location (cm^{-1})	Area						
0	1399	849	1421	3124	1445	8804	N/A	N/A	1455	7613
50	1402	1426	1426	9282	1448	7418	1452	4452	1462	3716
100	1401	3939	1418	17565	1448	11713	1452	12643	1462	4480
150	1400	7501	1418	17240	1448	16607	1452	19226	1462	3946
200	1401	11383	1418	20765	1448	16104	1452	15516	1462	3166
250	1401	9412	1418	21027	1448	17768	1451	14431	1462	3748
300	1401	8646	1418	21592	1448	17570	1451	13810	1462	3713

Table S3. Fit of Raman spectra for P3HT-F4TCNQ excited by 785 nm at 30°C

P3HT-F4TCNQ 30 °C										
Time doped (s)	Charged Disordered		Charged Ordered		Neutral Ordered		Dopant Anion		Neutral Disordered	
	Peak location (cm ⁻¹)	Area	Peak location (cm ⁻¹)	Area	Peak location (cm ⁻¹)	Area	Peak location (cm ⁻¹)	Area	Peak location (cm ⁻¹)	Area
0	1405	466	1424	1363	1445	5882	N/A	N/A	1462	2779
50	1401	1987	1421	6226	1448	7065	1452	5548	1462	2498
100	1400	2810	1418	8212	1448	7446	1452	7534	1462	2027
150	1401	4869	1418	12464	1448	8958	1451	7028	1462	2384
200	1404	3800	1418	17375	1448	8986	1451	6460	1462	1786
250	1401	4946	1418	15501	1448	11410	1451	7956	1462	2364
300	1401	5380	1418	15484	1448	13116	1451	9815	1462	2434

Table S4. Fit of Raman spectra for P3HT-F4TCNQ excited by 785 nm at 70°C

P3HT-F4TCNQ 70 °C										
Time doped (s)	Charged Disordered		Charged Ordered		Neutral Ordered		Dopant Anion		Neutral Disordered	
	Peak location (cm ⁻¹)	Area	Peak location (cm ⁻¹)	Area						
0	1399	849	1421	3124	1445	8804	N/A	N/A	1455	7613
50	1399	1900	1419	17045	1448	9123	1453	8345	1462	6847
100	1401	2683	1419	16482	1448	8792	1452	9769	1462	4378
150	1401	9834	1418	22668	1448	17533	1452	17262	1462	4892
200	1403	11449	1419	20304	1448	15440	1452	15663	1462	3516
250	1402	11606	1418	25765	1448	17284	1452	15923	1462	3971
300	1401	8614	1418	20075	1448	17337	1452	12929	1462	3863

References:

- 1 B. X. Dong, J. A. Amonoo, G. E. Purdum, Y.-L. Loo and P. F. Green, *ACS Appl. Mater. Interfaces*, 2016, **8**, 31144–31153.
- 2 J. Hynnen, D. Kiefer and C. Müller, *RSC Adv.*, 2018, **8**, 1593–1599.
- 3 J. Nightingale, J. Wade, D. Moia, J. Nelson and J.-S. Kim, *J. Phys. Chem. C*, 2018, **122**, 29129–29140.
- 4 T. Degouée, V. Untilova, V. Vijayakumar, X. Xu, Y. Sun, M. Palma, M. Brinkmann, L. Biniek and O. Fenwick, *J. Mater. Chem. A*, 2021, **9**, 16065–16075.
- 5 M. J. Dyson, E. Lariou, J. Martin, R. Li, H. Erothu, G. Wantz, P. D. Topham, O. J. Dautel, S. C. Hayes, P. N. Stavrinou and N. Stingelin, *Chem. Mater.*, 2019, **31**, 6540–6547.